RSC Advances

ROYAL SOCIETY OF CHEMISTRY

www.rsc.org/advances

RSC Advances RSCPublishing

ARTICLE

Tunable Band Gaps of $Co_{3-x}Cu_xO_4$ Nanorods with Various Cu Doping

Cite this: DOI: 10.1039/x0xx00000x

Chun-Te Ho, Tsu-Heng Weng, Chiu-Yen Wang, Shiang-Jie Yen and Tri-Rung Yew*

Received 00th January 2012,
Accepted 00th January 2012

DOI: 10.1039/x0xx00000x

www.rsc.org/

$Co_{3-x}Cu_xO_4$ nanorods with a crystalline structure, was synthesized via solution process in this study. The $Co_{3-x}Cu_xO_4$ nanorods exhibit dual direct bandgaps and could be adjusted at 1.3 - 1.5 eV, and 2.55 - 3.5 eV by using different Cu-doping concentrations. The $Co_{3-x}Cu_xO_4$ nanorods show an absorption coefficient of ~10^4 cm^{-1} and increases with the increase of Cu doping concentration.

Introduction

Cobalt oxide (Co_3O_4) based materials have been widely studied because of their potential applications in many technological fields. Especially, their applications in gas sensors[1,2], electrochromics devices[3], heterogeneous catalysts[4], high-temperature solar selective absorbers[5], electrocatalytic oxygen evolution reaction (OER)[6], supercapacitors[7], and lithium batteries[2,8,9] have been extensively investigated. These applications are mainly attributed to the high surface area and better electrochemical reactivity of nanostructured Co_3O_4.

Besides, there has been an increasing interest in developing metal-doped Co_3O_4, since the Co_3O_4 properties could be adjusted by the substitution of cobalt ions with foreign divalent metal ions in spinel structure. For example, Li- and Au- doped Co_3O_4 nanowires have been synthesized and exhibited a high storage capacity for lithium batteries[10]. There are a few studies focusing on Cu-doped Co_3O_4 recently[11]. The enhancement of Cu-doped Co_3O_4 in catalytic activity, OER[11], and the sensitivity of methane gas sensor[12] were reported in these studies.

In addition, to estimate the electronic structure and band gap value before and after doping metal, theoritical calculation has been made in previous literatures.[13-15]

In this study, efforts have been made to synthesize $Co_{3-x}Cu_xO_4$ nanorods by low temperature hydrothermal process. The morphology, structure and optical property with various Cu doping concentrations were characterized. In addition, the growth of $Co_{3-x}Cu_xO_4$ nanorods on conductive substrates have also been investigated for the future application on self-assembled electrical devices.

Experimental

Cu-doped Co_3O_4 nanostructure preparation[9]

$Co(NO_3)_2{\cdot}6H_2O$(0.1M) and Cu $(CH_3COO)_2{\cdot}3H_2O$ (0.02 M, 0.01 M, and 0 M) were loaded into a 500 ml reactor respectively, which was prefilled with 34 ml NH_4OH and 66 ml DI water. The reactor was put in a reflux system and remained at 85 ^oC for 12 hr, and then cooled down to room temperature. The reaction temperature and time have been optimized, which were presented in following paragraph. The final products were centrifuged and rinsed with distilled water and ethanol for several times to remove chemical residuals. After rinsing, the product was annealed in the furnace at 400 ^oC for 2 hr to ensure that other chemical residuals were completely eliminated.

Cu-doped Co_3O_4 nanorods optimization

The optimization of Co_3O_4 nanorods at various reaction temperatures and concentrations of reduction agent (ammonia), while all using 10 % molar ratio of $Cu(CH_3COO)_2$ in $Co(NO_3)_2$, were also investigated in this work as shown in Figure 1. It could be observed that different processing temperatures (60, 85, and 120 ºC) result in different surface morphology (Figure 1a - 1c). With processing temperature at 60 ºC, the Cu-doped Co_3O_4 nanoparticles with ~ 50 nm in diameter were observed (Figure 1a). When the processing temperature increases to 85 ºC, the Cu-doped Co_3O_4 nanorods were observed (Figure 1b). For the synthesis temperature up to 120 ºC, the Cu-doped Co_3O_4 particles with a diameter of 600 - 1000 nm were observed in Figure 1c. The synthesis using various NH_4OH concentrations for 12 hr at 85 ºC result in different morphologies as shown in Figures 1d - 1f. Figure 1d presents the Cu-doped Co_3O_4 nanoparticles with a diameter of 200 - 400 nm using H_2O to NH_4OH molar ratio 4:1. As the H_2O to NH_4OH molar ratio was decreased to 2:1, the Cu-doped Co_3O_4 nanorods were synthesized (Figure 1e). When the H_2O to NH_4OH molar ratio decreases to 1:1, the Cu-doped Co_3O_4 nanorods with slightly rough surface were observed (Figure 1f). As the nanorods morphology could provide larger surface area light collection, the optimized condition was determined to be at 85 ºC and H_2O to NH_4OH molar ratio 2:1.

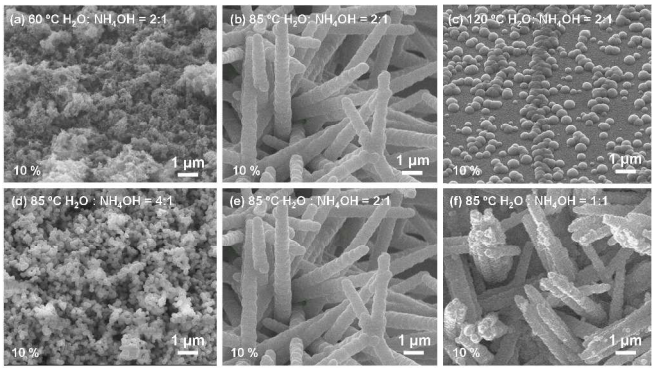

Fig 1. The SEM images of Cu-doped Co_3O_4 nanorods grown on Pt/glass substrates at the growth temperature of (a) 60 ºC, (b) 85 ºC, and (c) 120 ºC with H_2O: NH_4OH = 2:1 for 12 hr. The samples were prepared using (d) H_2O: NH_4OH = 4:1, (e) H_2O: NH_4OH = 2:1, and (f) H_2O: NH_4OH = 1:1 at a process temperature of 85 ºC for 12 hr. All above Cu-doped Co_3O_4 samples were, synthesized using 10 % molar ratio of $Cu(CH_3COO)_2$ in $Co(NO_3)_2$.

Materials characterization

The morphology and structure of the products were characterized by field emission scanning electron microscopy (FESEM, JOEL-JSM 6500F), high resolution transmission electron microscopy (HRTEM, JOEL-JSM 2010) and X-ray diffraction spectroscopy (Shimadzu XRD 6000). The compositions of the materials were analyzed by the inductively coupled plasma mass spectrometry (ICP-MS, PerkinElmer). Raman spectra (HORIBA HR 800, laser excitation λ = 633 nm) were accuqired to characterize the structural properties. The chemical composition of Cu-doped CO_3O_4 nanorods was characterized by X-ray photoelectron spectroscopy (XPS, PHI Quantera SXM). The optical properties were measured by an ultraviolet-visible near-infrared spectrophotometer (UV-Vis-NIR, Hitachi U-4100) over the range of 400 - 2000 nm, and a crygenic cathodoluminescence system (CL, Gatan MonoCL) at room temperature (~ 300 K) with an excitation beam with a 30 kV accelerating voltage and ~ 18 nA beam current.

Results and discussion

Morphology and structure analysis

The Cu-doped Co_3O_4 nanorods were synthesized by ammonia-evaporation-induced growth.[9] The glass substrates with and without a Pt layer were immersed in an aqueous solution with $Co(NO_3)_2$, and different amounts of $Cu(CH_3COO)_2$ were added into the solution to adjust the Cu-doping level in Co_3O_4 nanorods. The effects of process temperatures and NH_4OH concentrations on the morphology of Cu-doped Co_3O_4 nanorods were investigated. The results in Figure 1 show the optimum synthesis condition at H_2O: NH_4OH = 2:1 and a process temperature of 85 ºC for 12 hr, which will be used for further study. It could be observed that different concentrations of $Cu(CH_3COO)_2$ resulted in different Co_3O_4 surface morphologies as shown in the scanning electron microscopy (SEM) images of Figures 2a-2c. The pristine Co_3O_4 nanorods with about 200-500 nm in diameter, and 5-10 μm in length can be observed in SEM image (Figures 2a). With the increase of the molar ratio of $Cu(CH_3COO)_2$ in $Co(NO_3)_2$ from 10 % to 20 %, the corresponding diameter of Cu-doped Co_3O_4 nanorods increases from 300-600 nm to 500-800 nm as observed in the SEM images of Figures 2b and 2c, respectively.

The content of Cu in Co_3O_4 nanorods, synthesized by using 10 % molar ratio of $Cu(CH_3COO)_2$ in $Co(NO_3)_2$, were characterized by inductively coupled plasma mass spectrometry (ICP-MS spectrometer). The signal of Cu element (0.28 ± 0.01 at%) was measured in Co_3O_4 nanorods, which was calculated to be a compound of $Co_{2.98}Cu_{0.02}O_4$. The content of Cu in Co_3O_4 nanorods, synthesized by using 20 % molar ratio of $Cu(CH_3COO)_2$ in $Co(NO_3)_2$, were also characterized showing a Cu composition of 0.92 ± 0.02 at%, i.e., a compound of $Co_{2.94}Cu_{0.06}O_4$.

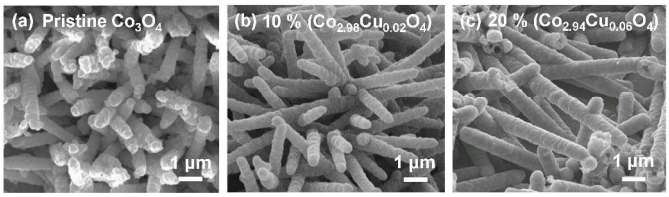

Fig 2. The SEM images of $Co_{3-x}Cu_xO_4$ nanorods grown on Pt/glass substrates (a) pristine Co_3O_4, (b) $Co_{2.98}Cu_{0.02}O_4$, and (c) $Co_{2.94}Cu_{0.06}O_4$.

The crystallographic properties of the $Co_{2.98}Cu_{0.02}O_4$ nanorods were examined by transmission electron microscopy (TEM), high-resolution TEM (HRTEM), and selected-area electron diffraction (SAED) as shown in Figures 3a-3d. The bright-field TEM image in Figure 3a reveals an individual $Co_{2.98}Cu_{0.02}O_4$ nanorod with a diameter of 200 nm. Figure 3b presents its dark field image contributed from the (111) diffraction of the $Co_{2.98}Cu_{0.02}O_4$. Figure 3c shows the corresponding diffraction pattern with the dotted ring-shaped patterns that indicate the polycrystalline structure of $Co_{2.98}Cu_{0.02}O_4$ nanorods. The d-spacings of 0.477 and 0.245 nm as calculated from the HRTEM lattice image of the $Co_{2.98}Cu_{0.02}O_4$ nanorods (Figure 3d) correspond to the spacing of 0.465 nm (111) and 0.243 nm (311), respectively, for the cubic spinel Co_3O_4 (a = 8.084 nm) according to X-ray JCPDS file No. 653103. It is interesting to observe the d-spacing is slightly larger than that of the JCPDS file reference, which suggests the doping of Cu atoms into Co_3O_4 nanorods lattice which leads to the expansion of Co_3O_4 lattice due to the larger size of Cu atom than Co.

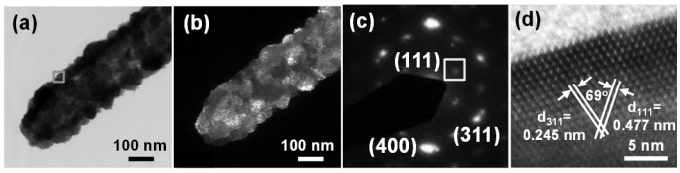

Fig 3. The transmission electron microscopy (TEM) analysis of $Co_{2.98}Cu_{0.02}O_4$. The (a) bright field image, (b) dark field TEM image contributed from (111) diffraction, (c) the corresponding diffraction pattern taken from (a), and (d) the high resolution TEM lattice image taken from the indicated boxed area of (c).

The crystal structure of Co_3O_4 nanorods with different amounts of Cu doping was also confirmed by X-ray diffraction spectroscopy (XRD), as shown in Figure 4a. It shows that for pristine Co_3O_4 nanorods all peaks can be indexed to cubic spinel phase Co_3O_4 based on the standard data file (JCPDS file No. 653103). It is intersting to obseve that the peaks shift to smaller-angles for both $Co_{2.98}Cu_{0.02}O_4$

and $Co_{2.94}Cu_{0.06}O_4$ compared to printine Co_3O_4. The peak shift indicates that the lattice is enlarged after Cu-doping in Co_3O_4, which is mostly due to the radius of Cu atom is larger than that of Co. The results are consistent with the lattice enlargement observed in the previous lattice image of HRTEM (Figure 3d).

The structure properties of pristine Co_3O_4, $Co_{2.98}Cu_{0.02}O_4$ and $Co_{2.94}Cu_{0.06}O_4$ were also analyzed by Raman spectra as shown in Figure 4b. The Co_3O_4 is belonged to spinel structure, $Co^{2+}(Co^{3+})_2(O^{2-})_4$, with space group O_h^7. Co^{3+} and Co^{2+} placed at octahedral and tetrahedral sites of Co_3O_4, respectively. The vibrational modes of Co_3O_4 at $k = 0$ in irreducible representations of the factor group O_h^7 are

$$\Gamma = A_{1g} + E_g + 3F_{2g} + 5F_{1u} + 2A_{2u} + 2E_u + 2F_{2u} \quad (1)$$

The A_{1g}, E_g and the three F_{2g} modes are Raman active. The F_{1g}, $2A_{2u}$, $2E_u$ and $2F_{2u}$ modes are inactive. In the five F_{1u} modes, one is an acoustic mode and the other four are infrared active.[16,17] In Raman spectra, the blueshift increases with the increase of Cu doping concentration in Co_3O_4 nanorods. The blueshift is believed to originate from the stress attributed to the lattice expansion.[18,19] It is again consistent with the observation of lattice image HRTEM. The corresponding Raman data and the comparison of their characteristics peaks are summarized in Table 1.

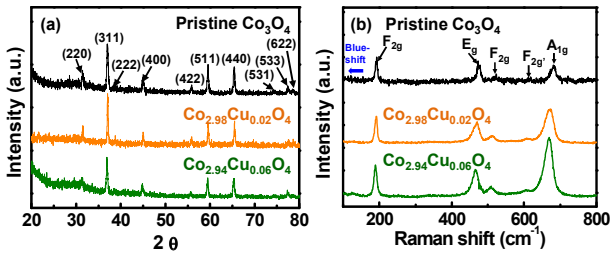

Fig 4. (a) XRD patterns of pristine Co_3O_4, $Co_{2.98}Cu_{0.02}O_4$ and $Co_{2.94}Cu_{0.06}O_4$ nanorods and b) their Raman spectra.

The purity and composition of Cu-doped Co_3O_4 nanorods were also analyzied using X-ray photoelectron spectroscopy (XPS), and the results show that the Cu has been doped into Co_3O_4 succesfully, including Cu^+ and Cu^{2+}, shown in Figure 5 and Table 2.

The full survey spectra of pristine Co_3O_4, $Co_{2.98}Cu_{0.02}O_4$ and $Co_{2.94}Cu_{0.06}O_4$ are presented in Figure 5a. The binding energy at 284.7 eV on the C 1s XPS spectrum corresponds to the carbon gel. The peaks located at 284.7, 532, and 780 eV are assigned to the characteristic peaks of C 1s, O 1s, and Co 2p, respectively. The peak located at 929 eV is assigned to Cu 2p, which becomes sharper at higher Cu doping concentration and confirms the existence of Cu in Co_3O_4. The further analysis of the $Co_{2.98}Cu_{0.02}O_4$ nanorods shows the peaks of Cu 2p, O 1s, and Co 2p (Figures 5b-d). Figure 5b shows the Cu 2p peaks at 927.6, 932.2, and 933.8 eV, which are attributed to multi-copper complex, Cu^+, and Cu^{2+}, respectively[20-22]. This reveals again that Cu has been doped into Co_3O_4 nanorods successfully, including Cu^+ and Cu^{2+}.

As expected in Figure 5c, the O 1s peaks at 529.9 and 532.4 eV can be assigned to Co_3O_4, and 531.2 and 534.3 eV to Cu_2O and CuO peaks, respectively. The representative XPS spectrum of Co 2p in Figure 5d shows that the peaks at 780.6, and 795.6 eV correspond to Co(III) $2p_{3/2}$ and $2p_{1/2}$, while 783.7 and 798.8 eV correspond to Co(II) $2p_{3/2}$ and $2p_{1/2}$, respectively. The weak $2p_{3/2}$ satellite features were found at 786.7 and 790 eV, and those of $2p_{1/2}$ satellite features were found at 802.6 and 805.8 eV[23-25], respectively. Based on above XPS characterization, the Cu-doping in Co_3O_4 nanorods were further confirmed. The XPS results are summarized in Table 2.

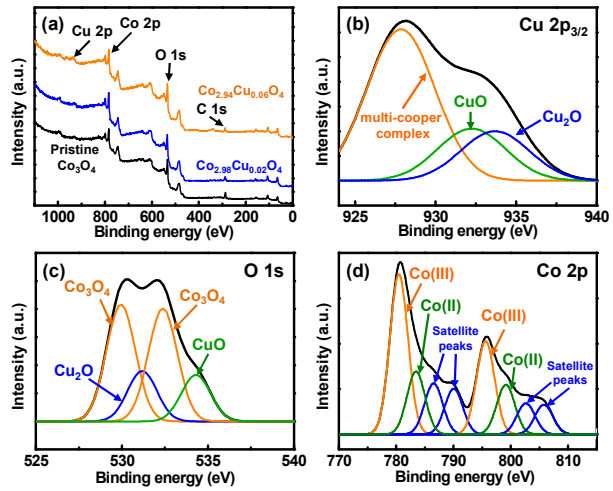

Fig 5. The XPS analyses show (a) the wide scan energy spectra of pristine Co_3O_4, $Co_{2.98}Cu_{0.02}O_4$ and $Co_{2.94}Cu_{0.06}O_4$, and the XPS spectra, including (b) Cu $2p_{3/2}$ spectrum, (c) O 1s spectrum, and (d) Co $2p_{3/2}$ and Co $2p_{1/2}$ spectra, for the $Co_{2.98}Cu_{0.02}O_4$ nanorods.

3.2. Optical property analyses

The optical properties of the Cu-doped Co_3O_4 nanorods were analyzed by UV-Vis and cathodoluminescence (CL) spectra. From the UV-Vis absorption spectra in Figure 6a for the pristine Co_3O_4, $Co_{2.98}Cu_{0.02}O_4$ and $Co_{2.94}Cu_{0.06}O_4$, it is noteworthy that the concentration of Cu dopant affects the absorption of nanorods significantly. In the visible light region, the absorption of Cu-doped Co_3O_4 nanorods increases with the increase of Cu dopant concentration. In order to quantify the enhancement of Cu-doping, the corresponding absorption coefficient was calculated according to Beer's law from different thicknesses of Cu-doped Co_3O_4. The absorption coefficients at 550 nm wavelength for the pristine Co_3O_4, $Co_{2.98}Cu_{0.02}O_4$ and $Co_{2.94}Cu_{0.06}O_4$ are 2.1 x 10^4, 3.1 x 10^4, and 4.5 x 10^4 cm^{-1}, respectively, which also increase with the increase of Cu dopant concentration. In addition, the optical band gaps of Cu-doped Co_3O_4 nanorods could be adjusted by varying the concentrations of Cu dopant. The pristine Co_3O_4 nanorods exhibit the band gaps of 1.4 and 3.5 eV. With the increase of Cu-doping, the band gaps shift to 1.35 and 2.75 eV for the $Co_{2.98}Cu_{0.02}O_4$ nanorods and to 1.3 and 2.5 eV for $Co_{2.94}Cu_{0.06}O_4$ nanorods. These values were extracted to the energy (= $h\nu$) axis at $\alpha = 0$ according to the linear portion of $(\alpha h\nu)^2$ - $h\nu$ plots, which were inserted in Figures 6b-6d, where α, h, and ν represent absorption coefficient, Plank constant, and wavelength, respectively[26,27].

The reason for band gap narrowing is beacuse Cu dopant replaces Co place and bonds with O. CuO and Cu_2O band gaps (~1.21 eV and ~2.10 eV, respectively) are smaller than Co_3O_4 band gaps (1.40 eV and 3.50 eV, respectively). Besides, Cu^+ and Cu^{2+} could occupy Co^{+2} or Co^{+3} place in Co_3O_4, which generates one more hole carriers.

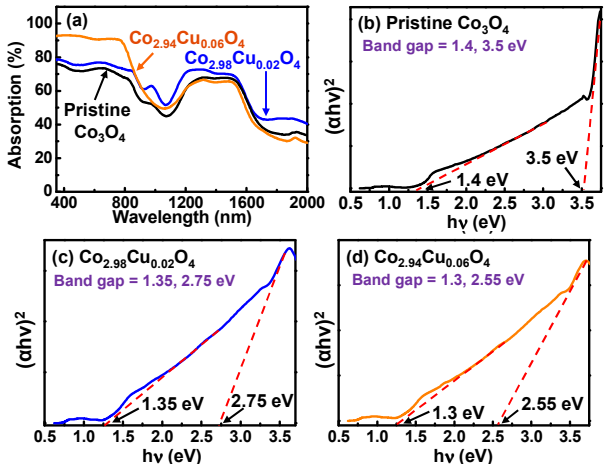

Fig 6. (a) UV-Vis absorption spectrum of the pristine Co_3O_4, $Co_{2.98}Cu_{0.02}O_4$ and $Co_{2.94}Cu_{0.06}O_4$ nanorods. Plots of $(\alpha h\nu)^2$ versus $h\nu$ show the direct band gap of (b) pristine Co_3O_4, (c) $Co_{2.98}Cu_{0.02}O_4$ and (d) $Co_{2.94}Cu_{0.06}O_4$ nanorods.

The absorption coefficient of ~ 10^4 cm^{-1} and direct band gaps of 1.4, 1.35, and 1.3 eV for Cu-doped Co_3O_4 nanorods suggest that they could serve as an efficient light harvesting agent for potential photovaltic and photodiode applications.

Their CL properties were determined in Figure 7a - 7c. The spectra are basically composed of two peaks and the left peak can be deconvoluted into two sub-peaks (peak 1 and peak 2). The Co_3O_4 absorption bands have been reported to be related to the ligand field transitions of Co^{3+} and Co^{2+} ions in octahedral and tetrahedral coordination, respectively, and the charge transfer process between Co^{2+} and Co^{3+} ions and those from oxygen ligands to Co ions[28]. The peak 1 and 2 are related to the transition between Co^{2+} and Co^{3+} bands, which are located at 2.5 - 2.9 eV and ~ 2.0 eV respectively. These peaks could correspond to the larger band gap transition in UV-Vis analyses. Comparing them with the UV-Vis band gap fitting results, the corresponding energies of these peaks are smaller than that of the larger band gap observed in UV-Vis analyses, which could be attributed to the deep-level emissions associated with defects[29]. The peak 3 could be corresponded to the band gap (~ 1.4 eV) transition of Cu-doped Co_3O_4 nanorods and it is consistent with the previous UV-Vis measurement. It is noteworthy that as the Cu-doping concentration increases, the peak 1 shifts to UV region while peak 2 and peak 3 shifts to infrared light region. The results and their comparison with other works are also summarized in Table 3 with the detailed analysis and description.

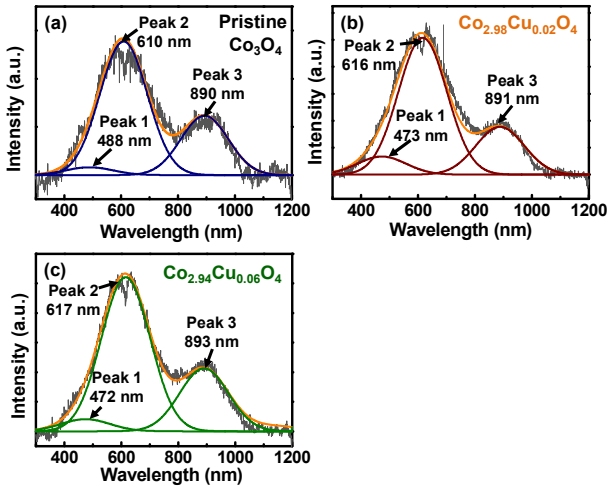

Fig 7. Cathodoluminescence (CL) spectra of (a) pristine Co_3O_4, (b) $Co_{2.98}Cu_{0.02}O_4$ and (c) $Co_{2.94}Cu_{0.06}O_4$ nanorods.

Conclusions

In summary, tunable band gaps of $Co_{3-x}Cu_xO_4$ nanorods, were synthesized via solution process and first reported in this study. Detailed characterizations of the nanorods show a crytalline structure and that the Cu has been doped into Co_3O_4 succesfully, including Cu^+ and Cu^{2+}. The optical properties were also carefully examined, showing that the absorption coefficient of nanorods increases with the increase of Cu dopant. The Cu-doped Co_3O_4 nanorods exhibit dual direct bandgaps and could be adjusted at 1.3 - 1.5 eV, and 2.55 - 3.5 eV by Cu-doping using different Cu-doping concentration (the higher the doping, the lower the band gap). The Cu-doped Co_3O_4 nanorods also reveal an absorption coefficient about 10^4 cm^{-1}, which suggests that they could serve as a light harvesting agent for potential applications in photovaltics and photodiodes.

Acknowledgements

This work was supported by National Science Council under project number NSC 100-2221-E-007-002-MY3. The authors thank C. H. Chen, Y. H. Chang, C. H. Hsu and S. Y. Wei at National Tsing-Hua University for optical property measurements. The authors also thank Prof. J. Y. Gan, C. N. Yeh, C. W. Juan, Y. J. Hong, and Y. M. Hsu for the discussion of the nanorod synthesis.

Notes and references

* Corresponding Author: Tri-Rung Yew, Department of Materials Science and Engineering, National Tsing-Hua University, Hsinchu, Taiwan 30013, E-mail: tryew@mx.nthu.edu.tw; Fax: +886-3-5722366; Tel: +886-936347230

1. J. Wollenstein, M. Burgmair, G. Plescher, T. Sulima, J. Hildenbrand, H. Bottner and I. Eisele, Sensor Actuat B-Chem, 2003, 93, 442-448.
2. W. Y. Li, L. N. Xu and J. Chen, Adv Funct Mater, 2005, 15, 851-857.
3. T. Maruyama and S. Arai, J Electrochem Soc, 1996, 143, 1383-1386.
4. L. H. Hu, Q. Peng and Y. D. Li, J Am Chem Soc, 2008, 130, 16136-+.
5. K. Chidambaram, L. K. Malhotra and K. L. Chopra, Thin Solid Films, 1982, 87, 365-371.
6. Y. G. Li, P. Hasin and Y. Y. Wu, Adv Mater, 2010, 22, 1926-+.

7. X. H. Xia, J. P. Tu, Y. J. Mai, X. L. Wang, C. D. Gu and X. B. Zhao, J Mater Chem, 2011, 21, 9319-9325.
8. X. W. Lou, D. Deng, J. Y. Lee, J. Feng and L. A. Archer, Adv Mater, 2008, 20, 258
9. Y. G. Li, B. Tan and Y. Y. Wu, Nano Lett, 2008, 8, 265-270.
10. F. Nobili, F. Croce, R. Tossici, I. Meschini, P. Reale and R. Marassi, J Power Sources, 2012, 197, 276-284.
11. Q. Zhang, Z. D. Wei, C. Liu, X. Liu, X. Q. Qi, S. G. Chen, W. Ding, Y. Ma, F. Shi and Y. M. Zhou, Int J Hydrogen Energ, 2012, 37, 822-830.
12. Z. Sheikhi Mehrabadi, A. Ahmadpour, N. Shahtahmasebi and M. M. Bagheri Mohagheghi, Physica Scripta, 2011, 84, 015801.
13. Run, L, Ying D. and Baibiao H. J. Phys. Chem. Lett. 2013, 4, 2223-2229.
14. Run, L. and Niall J. English., Phys. Rev. B 2011, 83, 155209-155213
15. Run, L. and Niall J. English., Chem. Mater. 2010, 22, 1626-1623.
16. Hadjiev, V. G.; Iliev, M. N.; Vergilov, I. V., J. Phys. C Solid State 1988, 21, (7), L199-L201.
17. Shirai, H.; Morioka, Y.; Nakagawa, I., J. Phys. Soc. Jpn. 1982, 51, (2), 592-597.
18. Cheng, B. C.; Xiao, Y. H.; Wu, G. S.; Zhang, L. D., Appl. Phys. Lett. 2004, 84, (3), 416-418.
19. Sharma, S. K.; Exarhos, G. J., Solid State Phenom. 1997, 55, 32-37.
20. Zarate, R. A.; Hevia, F.; Fuentes, S.; Fuenzalida, V. M.; Zuniga, A., J. Solid State Chem. 2007, 180, (4), 1464-1469.
21. Abelev, E.; Starosvetsky, D.; Ein-Eli, Y., Electrochimica Acta. 2007, 52, (5), 1975-1982.
22. Chang, J. P.; Zhang, Z.; Xu, H.; Sawin, H. H.; Butterbaugh, J. W., J. Vac. Sci. Technol. A 1997, 15, (6), 2959-2967.
23. Petitto, S. C.; Langell, M. A., J. Vac. Sci. Technol. A 2004, 22, (4), 1690.
24. He, T.; Chen, D. R.; Jiao, X. L.; Wang, Y. L.; Duan, Y. Z., Chem. Mater. 2005, 17, (15), 4023-4030.
25. Guo, W. L.; E, Y. F.; Gao, L.; Fan, L. Z.; Yang, S. H., Chem. Commun. 2010, 46, (8), 1290-1292.
26. H. Yamamoto, S. Tanaka and K. Hirao, J Appl Phys, 2003, 93, 4158-4162.
27. G. X. Wang, X. P. Shen, J. Horvat, B. Wang, H. Liu, D. Wexler and J. Yao, J Phys Chem C, 2009, 113, 4357-4361.
28. Llavona, A.; Diaz-Guerra, C.; Sanchez, M. C.; Perez, L., Mater. Chem. Phys. 2010, 124, (2-3), 1177-1181.
29. Z. G. Chen, J. Zou, G. Liu, F. Li, Y. Wang, L. Z. Wang, X. L. Yuan, T. Sekiguchi, H. M. Cheng and G. Q. Lu, ACS nano, 2008, 2, 2183-2191.

RSC Advances RSCPublishing

ARTICLE

Table 1. The summary of Raman analyses.

	F_{2g} (cm^{-1})	E_g (cm^{-1})	F_{2g} (cm^{-1})	$F_{2g'}$ (cm^{-1})	A_{1g} (cm^{-1})
Pristine Co_3O_4 (ref) [2]	194	482	521	618	691
Pristine Co_3O_4	194	477	520	616	686
$Co_{2.98}Cu_{0.02}O_4$	191	470	510	608	672
$Co_{2.94}Cu_{0.06}O_4$	189	466	509	606	670

Table 2. The summary of XPS

	Cu $2p_{3/2}$[20-22]			Co2p[23-25]			O 1s[20-25]			C 1s[20-25]
	CuO	Cu_2O	Cu Multi-complex	Co(III)	Co(II)	Satellite peaks	Co_3O_4	CuO	Cu_2O	C
This work	933.8 eV	932.2 eV	927.6 eV	780.4 eV ($2p_{3/2}$)	783.4 eV ($2p_{3/2}$)	786.7 eV	529.9 eV	534.3 eV	531.2 eV	284.7 eV
						790 eV				
				795.4 eV ($2p_{1/2}$)	798.8 eV ($2p_{1/2}$)	802.6 eV	532.4 eV			
						805.8 eV				
Reference	933.6 eV	932.5 eV	927.0 eV	779.7 eV	781.3 eV	786.3 eV	531.1 eV	533.0 eV	530.9 eV	284.7 eV
						788.2 eV				
				794.8 eV	796.8 eV	802.1 eV	532.2 eV			
						805.2 eV				

Table 3. The summary of CL analyses.

	Center of Peak 1 (nm)	Center of Peak 2 (nm)	Center of Peak 3 (nm)
Pristine Co_3O_4	488	610	890
$Co_{2.98}Cu_{0.02}O_4$	473	616	891
$Co_{2.94}Cu_{0.06}O_4$	472	617	893

Tunable Band Gaps of $Co_{3-x}Cu_xO_4$ Nanorods with Various Cu Doping

Chun-Te Ho, Tsu-Heng Weng, Chiu-Yen Wang, Shiang-Jie Yen and Tri-Rung Yew*

Department of Materials Science and Engineering, National Tsing-Hua University

[*] Prof. Tri-Rung Yew, PhD, Corresponding author,

Department of Materials Science and Engineering

National Tsing-Hua University

101, Sec. 2, Kuang-Fu Road

Hsinchu, Taiwan 30013
E-mail: tryew@mx.nthu.edu.tw

Graphical Abstract

Chun-Te Ho, Tsu-Heng Weng, Chiu-Yen Wang, Shiang-Jie Yen and Tri-Rung Yew*

RSC Advances **2014**

Tunable band gaps of $Co_{3-x}Cu_xO_4$ nanorods were synthesized with solution process and first report in this study.